Cargo recognition of Nesprin-2 by the dynein adapter Bicaudal D2 for a nuclear positioning pathway that is important for neuronal migration

Sivasankar Putta[$,1], Estrella D Rodriguez Castro[$,1], M. Yusuf Ali[$,2], Jose M Garcia Martin[1], Xiaoxin Zhao[1], Samantha Sylvain[1], Kathleen M Trybus[*,2] and Sozanne R Solmaz[*,1]

[1] Department of Chemistry, Binghamton University, PO Box 6000, Binghamton, NY 13902.

[2] Department of Molecular Physiology and Biophysics, University of Vermont, Burlington, VT 05405.

[$]First authors, equally contributed.

*Corresponding authors.

SRS: E-mail: ssolmaz@binghamton.edu

Phone: +1 607 777 2089

KMT: E-mail: Kathleen.Trybus@med.uvm.edu

Phone: +1 802-656-8750

ABSTRACT

Nesprin-2 is a subunit of LINC complexes, which span the nuclear envelope and have key roles in mechanotransduction and nuclear positioning during brain and muscle development. Nesprin-2 interacts with the plus-end directed motor kinesin-1 and the dynein adapter Bicaudal D2 (BicD2), which in turn recruits the minus-end directed motor cytoplasmic dynein to position the nucleus during neuronal migration of postmitotic neurons, but the molecular details of these interactions are elusive. Here we present a structural model of a minimal Nesprin-2/BicD2 complex. A structure prediction with a PAE score in the high confidence range was obtained from AlphaFold and experimentally validated by mutagenesis, binding assays and biophysical studies. The core of the binding site is formed by spectrin repeats of Nesprin-2, which form an alpha-helical bundle with the cargo-binding domain of BicD2. The minimal Nesprin-2 fragment also interacts robustly with full-length BicD2. The BicD2-binding site is separated by a ~65 residue intrinsically disordered linker from the LEWD sequence motif, that acts as kinesin-1 recruitment site, and we propose that both kinesin-1 and BicD2/dynein interact with Nesprin-2 simultaneously. We propose that structurally distinct interactions between BicD2 and its cargo adapters Nesprin-2, Nup358 and Rab6, as well as distinctions in the adjacent kinesin-1 recruiting sites could finetune overall motility for these transport pathways that have important roles in brain and muscle development. Mutations of Nesprin-2 and BicD2 cause devastating brain and muscle developmental diseases, including Emery-Dreifuss Muscular Dystrophy and spinal muscular atrophy, and results may help devise therapies for these diseases.

INTRODUCTION

Nesprin-2 is a subunit of LINC complexes (linker of nucleoskeleton and cytoskeleton) (McGee et al., 2006), which spans the nuclear envelope and has important roles in mechanotransduction and in positioning of the cell nucleus during brain and muscle development, involving the motors dynein, kinesin-1 and actomyosin (Arsenovic et al., 2016; Gonçalves et al., 2020; X. Zhang et al., 2009a, 2009b; Zhu et al., 2017). The important role of this protein in brain development is underscored by the fact that SYNE-null mice, which lack the gene encoding Nesprin-2, develop brains with lamination and neuronal migration defects (X. Zhang et al., 2009a). Furthermore, several human disease mutations of Nesprin-2 cause Emery-Dreifuss Muscular Dystrophy, involving heart defects and skeletal muscle wasting (Q. Zhang et al., 2007), highlighting the important roles of Nesprin-2 in muscle development (Wilson & Holzbaur, 2012, 2015).

Nesprin-2 spans the outer nuclear membrane and recruits actin filaments as well as the motors cytoplasmic dynein and kinesin-1, which in turn link it to the microtubules cytoskeleton. In LINC complexes, Nesprin-2 interacts with SUN domain proteins (Sad1-UNC-84 homology) that span the inner nuclear membrane and bind to chromatin in the nucleus (McGee et al., 2006). As a result, LINC complexes can act as a force transducer between the nucleoskeleton and the cytoskeleton. LINC complexes position the nucleus during cell migration, thereby facilitating several key developmental processes including neuronal migration of postmitotic neurons (Gonçalves et al., 2020). Nuclear positioning by Nesprin-2 and the motors BicD2/dynein and kinesin-1 is important for neuronal migration during brain development. Nesprin-2 binds to the dynein adapter protein Bicaudal D2 (BicD2), which in turn recruits the motor complex cytoplasmic dynein for positioning of the nucleus towards the minus-end of microtubules. In addition, Nesprin-2 has also has a LEWD sequence motif (Dodding et al., 2011), which acts as recruiting site for the plus-end directed microtubules motor kinesin-1 (Fridolfsson et al., 2010; Gonçalves et al., 2020; Wilson & Holzbaur, 2012, 2015; Zhu et al., 2017). Association of opposite polarity motors such as dynein and kinesin-1 via adapter proteins is a common theme in cellular transport and

likely serves to finetune motility, however, the details of the underlying molecular mechanisms are still unknown.

A second nuclear positioning pathway that is active at an earlier stage of brain development is facilitated by the recruitment of BicD2 to the nuclear pore protein Nup358 in G2 phase of the cell cycle (Hu et al., 2013; Splinter et al., 2010). This nuclear positioning pathway is essential for the differentiation of radial glial progenitor cells, which give rise to the majority of neurons and glia cells in the brain (Hu et al., 2013). Finally, BicD2 also interacts with Rab6^{GTP}, a key effector of protein secretion, to recruit motors for the transport of secretory and Golgi-derived vesicles, and several secreted protein factors have key roles in brain development (Brault et al., 2022; Grigoriev et al., 2007; Hoogenraad et al., 2003; Matanis et al., 2002; Serra-Marques et al., 2020; Zhao et al., 2024). The importance for BicD2-dependent cellular transport pathways in brain and muscle development is underscored by the fact that human disease mutations of BicD2 cause devastating brain and muscle developmental defects, including spinal muscular atrophy, the most common genetic cause of death in infants (Peeters et al., 2014; Rossor et al., 2020; Will et al., 2019; Yi et al., 2023). Several of the disease mutations cause changes in the affinity of BicD2 to distinct cargoes including Nup358, Nesprin-2 and Rab6^{GTP}, altering the associated cellular transport pathways (Yi et al., 2023). The cargo-binding domain of BicD2 is located in the C-terminal portion of coiled coil domain 3 (CC3) (Hoogenraad et al., 2001, 2003; Matanis et al., 2002). Rab6^{GTP}, Nesprin-2 and Nup358 bind to distinct but overlapping binding sites on BicD2 and compete, explaining the distinct effects of BicD2 mutations on the affinities towards these cargoes (Gibson et al., 2022, 2023; Noell et al., 2018; Yi et al., 2023; Zhao et al., 2024). This is also in line with the structural models of Rab6^{GTP}/BicD2 and Nup358/BicD2, which we have previously established and validated (Gibson et al., 2022, 2023; Zhao et al., 2024). In addition, several viruses and bacteria high-jack BicD2-dependent cellular transport pathways (Dharan et al., 2017; Manigrasso et al., 2024). However, a structural basis of how BicD2 recognizes its cargo adapter Nesprin-2 is elusive.

The recruitment site for dynein/BicD2 and kinesin-1 was previously mapped to residues 6123 - 6421 of mouse Nesprin-2, which includes spectrin repeats (SR) SR52, SR53 and the AD domain (Gonçalves et al., 2020; Yi et al., 2023; Zhu et al., 2017). With these results, a mini-Nesprin-2 was constructed, which fused the N-terminal actin-recruiting domain to the microtubules motor recruitment domain located in SR52 - SR56, followed by the transmembrane alpha-helix and the C-terminal KASH domain. While depletion of Nesprin-2 in rat embryo brains during development causes defects in neuronal migration, expression of the mini-Nesprin-2 restored near normal migration of neurons to the cortical plate. Deletion of the microtubules motor domain resulted in a 7-fold increase of the distance of the nucleus and the centrosome. These results suggest that the microtubules motor recruitment domain of Nesprin-2 has a key role in nuclear migration in neurons (Gonçalves et al., 2020).

Here, we establish a structural model of the minimal Nesprin-2/BicD2 complex, which includes the minimal microtubules motor recruitment domain of Nesprin-2, using structure prediction by AlphaFold. The core of the interaction is formed by SR repeats 52 and 53 of Nesprin-2, which form a helical bundle with the BicD2-CTD, although additional, weaker interfaces may be formed by adjacent domains. The model was validated by mutagenesis, binding assays and biophysical experiments. The BicD2/dynein binding site on Nesprin-2 is spatially close but does not overlap with the LEWD sequence motif that acts as kinesin-1 binding site. These results suggest that the opposite polarity motors dynein and kinesin-1 may interact simultaneously with Nesprin-2/BicD2 to facilitate a nuclear positioning pathway during neuronal migration.

RESULTS

A structural model of the minimal Nesprin-2/BicD2 complex with a PAE score in the high confidence range was obtained using AlphaFold

BicD2 recruits dynein, dynactin and kinesin to the cargo adapter and LINC complex component Nesprin-2, for a nuclear positioning pathway that is important for muscle development and

neuronal migration, a fundamental process in brain development (Gonçalves et al., 2020). We have previously reconstituted a recombinant minimal Nesprin-2-min/BicD2-CTD complex (Yi et al., 2023), with the C-terminal cargo binding domain (CTD) of human BicD2 (aa 715 - 804) and spectrin repeats (SR) SR52 and SR53 of Nesprin-2 (aa 6123 to 6421). This Nesprin-2 domain has been previously mapped as the minimal recruiting domain for dynein and kinesin-1 (Gonçalves et al., 2020; Zhu et al., 2017). To establish a structural basis for the interaction of the dynein adapter BicD2 with Nesprin-2, we predicted the structure of this minimal complex with Colabfold (Mirdita et al., 2022), which implements the AI-based structure prediction software AlphaFold (Evans et al., 2022; Jumper et al., 2021). A complex with a 2:2 stoichiometry was predicted, as two BicD2/cargo complexes (Nup358/BicD2 and Rab6^{GTP}/BicD2) were previously characterized by size exclusion chromatography coupled with multi-angle light scattering and small-angle X-ray scattering, which established a 2:2 stoichiometry for these complexes (Cui et al., 2019; Gibson et al., 2022; Noell et al., 2018). Furthermore, the X-ray structure of the C-terminal cargo-binding domain (CTD) of human BicD2 was previously determined, which confirmed that BicD2 forms a homo-dimer (Noell et al., 2018, 2019).

The structural model of this minimal Nesprin-2/BicD2 complex (termed Nesprin-2-min/BicD2-CTD) with the lowest predicted aligned error (PAE) is shown in Fig. 1, and the remaining predicted models and their respective PAE plots are shown in Fig. S1. These predictions are overall quite similar. In the structural model, spectrin repeats SR52 and SR53 of Nesprin-2, which each consist of three alpha-helices form a helical bundle with the BicD2-CTD. The spectrin repeats are followed by the intrinsically disordered AD domain, which includes the sequence motif LEWD that recruits kinesin-1. This intrinsically disordered domain does not engage in the interaction with BicD2 in the structural model.

A key metric for evaluation is the predicted aligned error (PAE), as it provides an error estimate for the distances of each residue pair within the predicted structure. The PAE of the highest-ranking model is mostly below 5 - 10 Å, reflecting a high degree of confidence in the predicted

structure of the minimal Nesprin-2-min/BicD2-CTD complex (Fig. 1B). The only region with a higher PAE error is the intrinsically disordered AD domain, as to be expected for a disordered domain. This region also does not engage in the interaction with BicD2-CTD.

The predicted local distance difference test (pLDDT), is a per-residue metric of local confidence. It estimates how well the predicted structure would agree with an experimental structure based on a local distance difference test. The pLDDT scores for all predicted models are above 80 - 98, suggesting that they are reliable. It should be noted that the intrinsically disordered AD domain of Nesprin-2 that does not interact with BicD2, as well as a few other residues have low pLDDT scores, as expected for disordered domains (Fig. S1).

Furthermore, we also predicted the structure of a larger 2:2 complex including spectrin repeats SR48 - SR53 of Nesprin-2 (aa 5692 - 6342) and the entire coiled coil 3 domain of human BicD2 (aa 667-804). This larger complex was chosen based on recent results suggesting that inclusion of spectrin repeat SR48 increased the interaction of Nesprin-2 with BicD2 based on qualitative binding assays (Zhou et al., 2024). Figure 2 shows the highest-ranking model from the structural prediction of this larger complex. A least square superimposition of the structural models of the larger complex with Nesprin-2 SR48 – SR53 and BicD2-CC3 and the minimal Nesprin-2-min/BicD2-CTD complex suggests that they are very similar in the shared domains, supporting that the structural model of the minimal complex is reliable, since the addition of the additional regions does not significantly change the structure prediction of the minimal complex. However, the PAE plot of the larger complex indicates a high error for the additional domains, suggesting that the structure prediction of the added domains is not reliable. In addition, the five highest-ranking models from the structure prediction of the larger complex are very different from each other, despite promising pLDDT scores in the reliable range (Fig. S2). Due to the high PAE errors and the differences of the predictions, we concluded that only the structure prediction of the minimal Nesprin-2-min/BicD2-CTD complex was reliable. Thus, we focused in the subsequent structural analysis on the minimal Nesprin-2-min/BicD2-CTD complex. It should be noted that

additional, weaker interfaces between Nesprin-2 and BicD2 may be formed in the context of the full-length proteins.

Validation of the structural model of the Nesprin-2/BicD2-CTD complex

To validate the structural model of the Nesprin-2-min/BicD2-CTD complex, we designed a series of deletion constructs of Nesprin-2-min and assessed binding to BicD2-CTD by GST-pulldown assays (Fig. 3). Three constructs were designed to consecutively delete portions of the intrinsically disordered AD domain, which does not engage in the interaction with BicD2 in the structural model of the Nesprin-2-min/BicD2-CTD complex. The minimal Nesprin-2 deletion construct that still bound robustly to BicD2-CTD in the pulldown assays (aa 6123 - 6340) lacked the entire intrinsically disordered domain (Fig. 3). These experiments suggest that the entire intrinsically disordered AD domain is dispensable for BicD2-CTD binding, in line with our structural model. Of note, this domain includes the LEWD sequence motif that acts as binding site for the kinesin-1 light chain 2 (Fig. 3), suggesting that BicD2/dynein and kinesin-1 may simultaneously bind to Nesprin-2.

An additional N-terminal deletion construct was designed to remove spectrin repeats SR52 and SR53. As expected, this construct did not pull down visible amounts of BicD2-CTD (Fig. 3).

To further validate our structural model of the Nesprin-2-min/BicD2-CTD complex, we also mutated contact residues of Nesprin-2 and BicD2 (Table S1) from the structural model to alanine and assessed binding of the mutants by GST-pulldown assays (Fig. 4). The elution fractions of the pulldown assays were analyzed using SDS-PAGE, and the ratio of bound Nesprin-2/BicD2-CTD was quantified from the intensity of the gel bands (Fig. 4). Several Nesprin-2 mutants had reduced expression and were excluded from the analysis as they may be misfolded. Five mutants of BicD2-CTD were identified, which reduced binding to Nesprin-2 (red in Fig. 4). These mutants were located in the extreme C-terminus of the BicD2-CTD, which was previously mapped as minimal Nesprin-2 binding site (Yi et al., 2023). The structural model of the minimal Nesprin-

2/BicD2 complex suggests that the core of the BicD2 binding site is formed by spectrin repeats SR52 and SR53 of Nesprin-2. Especially SR53 mediates many contacts with BicD2 and is likely the most important domain for the interaction. Five Nesprin-2 mutants (V6246, E6250, H6260, V6323, and R632) were identified, that displayed reduced binding to BicD2-CTD (red in Figure 4). Of note, a triple mutant (V6246A/L6253A/F6261A) was designed to disrupt three key hydrophobic contacts between Nesprin-2 and BicD2 that span most of the spectrin repeat SR53 (Fig. S3). This mutant virtually abolishes the interaction between Nesprin-2-min and BicD2-CTD in pulldown assays and was chosen for further characterization.

To exclude that these mutations result in structural changes or misfolding of Nesprin-2-min, which could result in reduced binding, even if the mutated residues were not engaged in the interaction, we assessed the secondary structure of Nesprin-2-min and the mutants by circular dichroism (CD) spectroscopy (Fig. 5). Representative CD wavelength scans of four mutants with reduced binding to BicD2 are shown in Fig. 5, overlaid with CD wavelength scans of WT Nesprin-2-min. Two local minima (at 208 nm and 222 nm) are observed for WT Nesprin-2-min, which are characteristic for alpha-helical structures. The wavelength scans of all four mutants are very similar to the wavelength scan of WT Nesprin-2-min (the experimental error of the molar ellipticity is 3.5 - 5% (Cui et al., 2020; Gibson et al., 2022)), suggesting that the mutations do not result in misfolding or large structural changes compared with the WT. These results validate the mutated residues with reduced binding as bona fide contact residues.

Fig. 4B shows a closeup of the interface between Nesprin-2 and BicD2-CTD, in which the residues that were confirmed to be important for the interaction by pulldown assays are shown in stick representation and labelled. Most of the confirmed Nesprin-2 contact residues are hydrophobic, whereas some of the BicD2 contact residues are also charged.

Notably, mutagenesis confirmed several residues to be essential for the Nesprin-2/BicD2 interaction, thereby validating our structural model of the Nesprin-2-min/BicD2-CTD complex. The structural model was also validated by deletion constructs which established that the intrinsically

disordered AD domain is dispensable for the interaction, in line with our structural model. The core of the binding site is formed by spectrin repeats SR52 and SR53, which form an alpha-helical bundle with the coiled-coil of the BicD2-CTD.

Comparison of the structural models of three BicD2/cargo complexes that are important for brain development

In addition to the structural model of the minimal Nesprin-2/BicD2 complex presented here, structural models for minimal Nup358/BicD2 and Rab6/BicD2 complexes were previously obtained from AlphaFold and validated through experiments (Gibson et al., 2022, 2023; Zhao et al., 2024). These experiments suggest that the three cargoes Nesprin-2, Nup358 and Rab6^{GTP} bind to distinct but overlapping binding sites on BicD2, which is in line with our previous results that these cargoes compete for binding (Noell et al., 2018; Yi et al., 2023). It is also in line with the distinct effects of human BicD2 disease mutations on the affinity of distinct cargoes (Fig. 6, Fig. S4, Fig. S5) (Yi et al., 2023).

The Nesprin-2-min/BicD2-CTD complex forms an alpha-helical bundle, in which SR52 and SR53 bind to Bic2D-CTD. The BicD2 binding site is succeeded by a ~65 residue intrinsically disordered domain followed by a LEWD motif that acts as recruitment site for kinesin-1 light chain 2. Thus, the recruitment sites for dynein/BicD2 and kinesin-1 are spatially close but do not overlap, suggesting that the opposite polarity motors dynein and kinesin-1 may potentially be recruited simultaneously to Nesprin-2.

The Nup358/BicD2 complex is structurally distinct, but similarly as in the Nesprin-2/BicD2 complex, the BicD2 binding site of the Nup358/BicD2 complex is followed by a ~30 residue intrinsically disordered domain and the LEWD motif (Fig. 6) (Cui et al., 2019; Gibson et al., 2022, 2023). While the overall architecture is similar, the intrinsically disordered domain between the BicD2 binding site and the LEWD motif is shorter for Nup358/BicD2 compared to Nesprin-2/BicD2. The minimal BicD2 binding site on Nup358 is structurally distinct from Nesprin-2/BicD2

and formed by a cargo-recognition alpha-helix, which binds to the center of the BicD2-CTD. This alpha-helix is intrinsically disordered in apo-Nup358 and folds to an alpha-helix upon binding to BicD2-CTD (Gibson et al., 2022, 2023).

We also carried out CD spectroscopy, to assess if the alpha-helices of the spectrin repeats SR52 and SR53 are already present in apo-Nesprin-2 or whether they only fold upon binding to the BicD2-CTD (Fig. S6). For these experiments, Nesprin-2-min and BicD2-CTD were mixed to assemble the complex, and CD wavelength scans were recorded. In addition, CD wavelengths scans of the individual proteins at the same concentration were recorded and the molar ellipticities of the two spectra were added together. The CD wavelength scan of the complex is very similar to the sum of the CD wavelength spectra of the individual proteins (Fig. S6). Both show comparable minima at 208 and 222 nm, which are characteristic for alpha-helical structures. The experimental error of the CD measurements is 3.5% at 208 nm and 5.2% at 222 nm (Cui et al., 2020; Gibson et al., 2022). These results suggest that the minimal Nesprin-2-min/BicD2-CTD complex has a similar alpha-helical content compared to the individual proteins, suggesting that there are no large structural changes such as the folding of additional alpha-helices during complex formation as observed for the Nup358/BicD2 complex (Gibson et al., 2022).

Finally, in the Rab6^{GTP}/BicD2 complex, Rab6^{GTP} binds to the extreme C-terminal region of the BicD2-CTD (Fig. 6, Fig. S6), which is structurally distinct from the Nup358/BicD2 and Nesprin-2/BicD2 complex. In contrast to Nup358 and Nesprin-2, Rab6^{GTP} lacks a known kinesin-1 recruitment site. However, kinesin-1 in all three BicD2/cargo complexes is still recruited to the coiled-coil domain 2 of BicD2 (Grigoriev et al., 2007), which binds to the kinesin-1 heavy chains. The interaction between BicD2 and cargoes is important to activate dynein for processive motility, and the observed structural differences of BicD2/cargo complexes could have implications on overall motility of the associated dynein and kinesin-1 motors.

Nesprin-2 fragments interact with full-length BicD2

We also probed the interaction of the minimal Nesprin-2 fragment to full-length BicD2, using single-molecule binding assays (Fig. 7). In these experiments, full-length BicD2 colocalized with the minimal Nesprin-2 fragment, confirming a robust interaction. In the absence of cargo, BicD2 forms an auto-inhibited, looped conformation. Binding of cargo such as the Nesprin-2 fragment, is expected to result in opening of the looped conformation, thereby making the N-terminal dynein/dynactin binding site accessible for motor recruitment (McKenney et al., 2014; Schlager et al., 2014).

DISCUSSION

Here we present a structural model of a minimal Nesprin-2/BicD2 complex that is based on a structure prediction by AlphaFold and experimentally validated by mutagenesis and binding assays. The core of the binding site is formed by spectrin repeats SR52 and SR53 of Nesprin-2 which form an alpha-helical bundle with the cargo-binding domain of BicD2. The spectrin repeats are followed by a ~65 residue intrinsically disordered domain, which includes the LEWD motif, that acts as kinesin-1 recruitment site. This disordered domain is dispensable for the interaction with the BicD2-CTD, suggesting that both kinesin-1 and BicD2/dynein may potentially interact with Nesprin-2 simultaneously, similar as for Nup358/BicD2/kinesin-1 (Cui et al., 2019). We also show that the minimal Nesprin-2 fragment interacts robustly with full-length BicD2. In a competition assay, this minimal Nesprin-2 fragment outcompetes Nup358 for binding to BicD2-CTD, suggesting that it has a higher affinity (Yi et al., 2023). A recent paper reported that additional regions of Nesprin-2, notably spectrin repeat 48, markedly increased the affinity of BicD2 to Nesprin-2 (Zhou et al., 2024), which is not present in our minimal Nesprin-2 fragment. It should be noted that while depletion of Nesprin-2 causes defects in neuronal migration in rat embryo brains, expression of a mini-Nesprin-2 that included the microtubules motor recruitment domain (SR52-SR56) but lacked SR48 restored near normal migrations of neurons in the cortical plate, suggesting that SR48 is dispensable for the recruitment of kinesin-1 and dynein to Nesprin-

2 (Gonçalves et al., 2020). Furthermore, we show that the minimal Nesprin-2 fragment composed of SR52 and SR53 robustly interacts with full-length BicD2. Full-length BicD2 forms a looped, auto-inhibited conformation that does not interact with dynein/dynactin. Binding of cargo activates full-length BicD2 for dynein and dynactin recruitment, and cargo-loaded adapters such as BicD2 are required for activation of processive motility (McKenney et al., 2014; Schlager et al., 2014). We have shown previously that specific interactions between Nup358/BicD2 and Rab6/BicD2 are important for overall motility of the recruited dynein complexes. Differences in speed and run length were observed for Nup358 mutants that disrupted the interaction with BicD2 (Gibson et al., 2022; Zhao et al., 2024), suggesting that structurally distinct BicD2/cargo interactions may modulate overall motility in cellular transport pathways.

The structural model of the minimal Nesprin-2/BicD2 complex is structurally distinct from other BicD2/cargo complexes but shares the LEWD motif with Nup358. The LEWD motif is located in an intrinsically disordered domain C-terminal of the BicD2 binding site. We show that this disordered domain with the LEWD motif is dispensable for BicD2 binding, whereas a recent study indicated that the mutation of the LEWD motif of Nesprin-2 to LEAA diminished binding to BicD2 in a pulldown assay that included cell extracts (Gonçalves et al., 2020). It remains to be established whether differences in the experimental setup, such as the presence of additional protein factors (e.g. kinesin-1) result in enhanced binding of BicD2 to Nesprin-2-LEWD versus Nesprin-2-LEAA. It should be noted that the intrinsically disordered linker between the BicD2 binding site and the LEWD motif is substantially longer for Nesprin-2/BicD2 compared with Nup358/BicD2 (~65 versus ~30 residues) which may have impacts on the overall motility. In contrast, Rab6 lacks a known kinesin-1 recruiting site. In all three BicD2/cargo complexes, the kinesin-1 heavy chain is also recruited via the coiled-coil 2 domain of BicD2 (Grigoriev et al., 2007). The observed structural differences of the BicD2/cargo interactions as well as the observed distinctions in the adjacent kinesin-1 recruiting sites could finetune overall motility of the recruited dynein and kinesin-1 complexes. While in the Nup358/BicD2 and Nesprin-2/BicD2 transport

pathways, dynein is the dominant motor, with kinesin-1 actively modulating the overall minus-end directed movement (Gonçalves et al., 2020; Hu et al., 2013; Splinter et al., 2010; Zhu et al., 2017), kinesin-1 is the dominant motor of the Rab6/BicD2 transport pathway, with dynein modulating overall plus-end directed motility (Serra-Marques et al., 2020). How overall directionality in such multi-motor complexes is achieved remains to be established.

Several disease mutations that cause brain and muscle developmental diseases in infants, including spinal muscular atrophy, are located in the cargo binding domain of BicD2. We have previously shown that several of the disease mutations affect the affinity of BicD2 towards Nesprin-2, Nup358 and Rab6 in a distinct manner, thereby modulating associated cellular transport pathways that are important for brain development (Yi et al., 2023). These results are in line with our structural models of three BicD2/cargo complexes, according to which Nesprin-2, Nup358 and Rab6 bind to overlapping but distinct sites on BicD2 (Cui et al., 2020; Zhao et al., 2024) (Fig. 6, Fig. S5).

METHODS

Structure predictions

The structure predictions were carried out using ColabFold v1.5.5 (Mirdita et al., 2022) with the Google Colab AlphaFold2_mmseq2 Notebook (https://colab.research.google.com/github/sokrypton/ColabFold/blob/main/AlphaFold2.ipynb, accessed on 19 March 2025), which implements AlphaFold (Evans et al., 2022; Jumper et al., 2021). Default settings were used; a template was not applied. A 2:2 hetero-dimer composed of two molecules of human BicD2 (aa 715 - 804 or aa 667 - 804) and two molecules of mouse Nesprin-2 (Uniprot ID Q6ZWQ0|) (aa 6123 - 6421 or aa 5692 - 6342) (Mirdita et al., 2022; Yi et al., 2023; Zhou et al., 2024; Zhu et al., 2017) was predicted. UCSF ChimeraX was used to create structure figures (Pettersen et al., 2021). The PISA server was used to identify contact residues between Nesprin-2 and BicD2 (Krissinel & Henrick, 2007).

GST-pulldown assay

All expression vectors were obtained from the company Genscript that performed gene synthesis of codon-optimized inserts, cloning and mutagenesis. Expression constructs of GST-tagged mouse Nesprin-2-min (aa 6123 – 6421, Uniprot ID Q6ZWQ0|) in the pGEX6p1 expression vector and his_6-tagged human BicD2-CTD (aa 715 - 804) in the pET28a expression vector were previously described (Noell et al., 2019; Yi et al., 2023). Mutagenesis was performed by Genscript. These protein fragments were expressed in *E. coli* and purified as previously described (Yi et al., 2023). GST pulldowns with GST-tagged Nesprin-2-min and BicD2-CTD fragments (WT, mutants or deletions) were performed as described (Yi et al., 2023). The background subtracted intensities of the gel bands corresponding to the Nesprin-2 and BicD2 fragments were quantified using ImageJ (Schneider et al., 2012) as described by (Yi et al., 2023). The ratio of bound BicD2-CTD/Nesprin-2-min was calculated and normalized to the WT (WT = 1).

Circular Dichroism (CD) spectroscopy

CD spectroscopy was performed as described (Zhao et al., 2024). For these experiments, GST-tagged Nesprin-2-min (aa 6123 – 6421) fragments (WT and mutants) were expressed and purified as described (Yi et al., 2023). The purified proteins were transferred into a buffer of 10 mM Tris, pH 8.0, 150 mM NaCl, 0.2 mM TCEP by three cycles of dilution and concentration in a centrifugal concentration filter as described (Zhao et al., 2024). The proteins were concentrated to 0.5 mg/ml unless otherwise noted. The protein concentration was determined by absorbance spectroscopy at 228.5 nm and 234 nm using the extinction coefficient of the peptide bond and flash-frozen in liquid nitrogen as described (Gibson et al., 2022).

CD measurements were recorded at a temperature of 10°C with the use of Jasco J-1100 CD spectrometer including CD, HT, and absorbance signals at a wavelength range of 250 to 190 nm. A quartz cuvette with a pathlength of 1 mm was used. The following parameters were used: data

pitch: 0.1 nm; D.I.T.: 2 s; bandwidth: 1.00 nm; scanning speed: 50 nm/min; 8 accumulations per sample. The wavelength scan of the buffer was subtracted from the recorded CD wavelength scans, and the raw ellipticity Θ (mdeg) was converted to mean residue molar ellipticity [Θ] (path length: 1 mm; number of peptide bonds: 542; molar mass (WT): 63,531.5 Da). The protein concentration used for the calculation was determined from the sample absorbance at 214 nm, after subtracting the buffer baseline, using the following extinction coefficients that were calculated with BeStSel (Micsonai et al., 2022): Nesprin-2 WT: 1199515 M^{-1} cm^{-1}; Nesprin-2/V6246A/L6253A/F6261A mutant: 1194323 M^{-1} cm^{-1}; V6246A mutant: 1199504 M^{-1} cm^{-1}; E6250A mutant: 1199469 M^{-1} cm^{-1}; H6260A mutant: 1194422 M^{-1} cm^{-1}. For each protein, two CD wavelength scans were recorded from separate purifications, and a representative result is shown.

Single molecule binding assays with Nesprin-2 and full-length BicD2

Nesprin-2 fragments (aa 6123 - 6352) were expressed and purified as N-terminal GST fusion proteins with C-terminal biotin-tag and flag-tag as described (Yi et al., 2023), using glutathione affinity chromatography and size exclusion chromatography with the Superdex 200 Increase 10/300 GL column (GE Healthcare), which was equilibrated with the following buffer: 20 mM HEPES pH 7.4, 150 mM NaCl, 0.5 mM TCEP . Full-length BicD2 was expressed and purified with N-terminal biotin tag as described (Gibson et al., 2022). These proteins were diluted to 2 μM in BRB80 buffer. BicD2 was incubated with streptavidin-conjugated Alexa Fluor 647, and Nesprin-2 was incubated with streptavidin-conjugated Alexa Fluor 488, each at a 1:1 molar ratio in separate tubes. After incubation on ice for 20 minutes, the two mixtures were combined to allow BicD2 and Nesprin-2 to interact. The resulting mixture was diluted 400-fold (final concentration: 1.25 nM) and introduced into a flow cell for imaging using TIRF microscopy. Alexa Fluor 488 was excited with a 488 nm laser, and Alexa Fluor 647 with a 640 nm laser.

ACKNOWLEDGEMENTS

SR Solmaz was supported by NIH grant R01 GM144578. The CD instrument was supported by NIGMS grants 1R01GM125853-02S1 and 3R35GM130207-01S1.

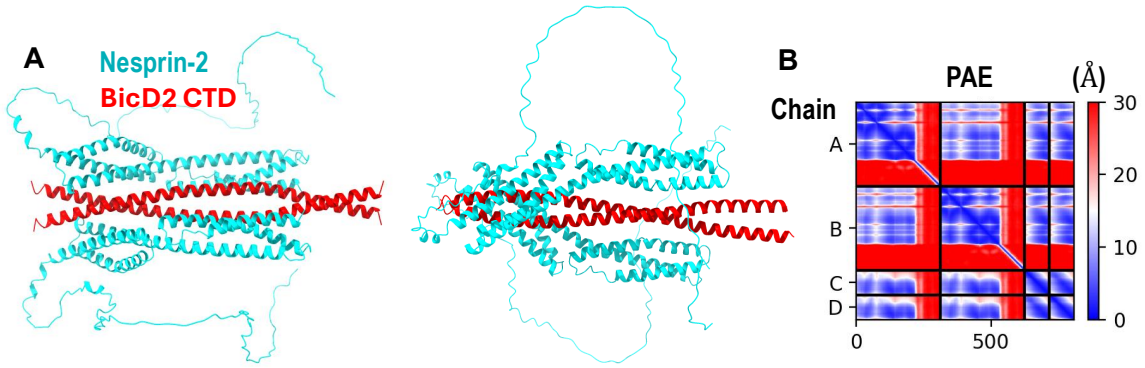

Fig. 1. A structural model of the minimal Nesprin-2/BicD2 complex with a reliable PAE score was obtained from AlphaFold. (A) Structural model of the minimal Nesprin-2/BicD2 complex from AlphaFold, shown in cartoon representation, rotated by 90°. (B) Predicted aligned error (PAE) plot for the highest-ranking model. The x and y axes show the residue numbers, starting with Nesprin-2 (aa 6123 – 6421, Chain A, B), followed by BicD2 (aa 715-804; chain C, D) (Gonçalves et al., 2019; Yi et al., 2023; Zhu et al., 2017). Additional models and error plots are shown in Fig. S1.

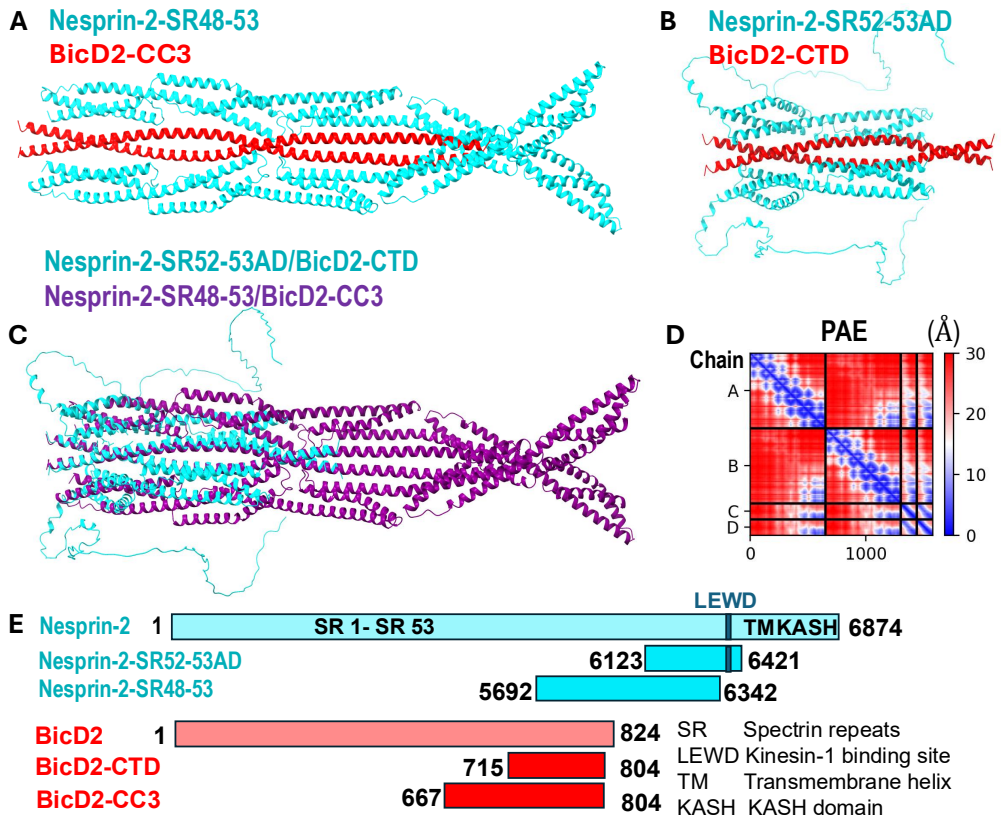

Fig. 2. The predicted structure of a larger Nesprin-2/BicD2 complex including spectrum repeats 48-58 and the entire coiled coil 3 of BicD2 is in line with the predicted structure of the minimal complex. (A) Structural model of a larger Nesprin-2/BicD2 complex (Nesprin-2 aa 5692-6342 (Zhou et al., 2024) and BicD2 aa 667-804) from AlphaFold, shown in cartoon representation. (B) Structural model of the minimal complex (Nesprin-2 aa 6123-6421 and BicD2 aa 715-804). (C) Least squares superimposition of A (purple) and B (cyan). Note that the predicted structure of the minimal complex closely resembles the predicted structure of the same domains in the context of the larger complex. (D) Predicted aligned error (PAE) plot for the hightest-ranking model. The x and y axes show the residue numbers, starting with Nesprin-2 (Chain A, B), followed by BicD2 (Chain C, D). Additional models and error plots are shown in Fig. S2. (E) Schematic representation of the Nesprin-2 and BicD2 fragments used for A and B (Yi et al., 2023; Zhou et al., 2024; Zhu et al., 2017).

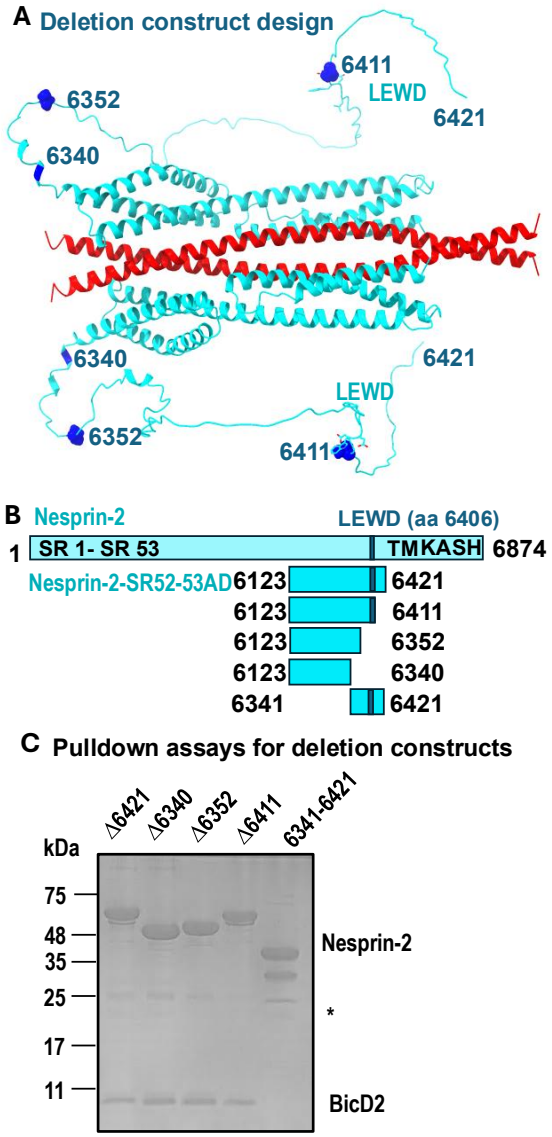

Fig. 3. The intrinsically disordered domain with the LEWD sequence motif that acts as kinesin-1 binding site is dispensable for the interaction with BicD2. (A) Structural model of the minimal Nesprin-2/BicD2 complex. The residue numbers for deletion sites are highlighted in dark blue and labelled. The LEWD motif is shown in stick representation. (B) Schematic representation of the deletion constructs. (C) Pulldown assays were conducted with the GST-tagged Nesprin-2 deletion constructs from B and BicD2-CTD. The SDS-PAGE of the elution fractions is shown. Note that all C-terminal deletions still interact with BicD2-CTD, suggesting that the intrinsically disordered regions with the LEWD motif are dispensable for the interaction.

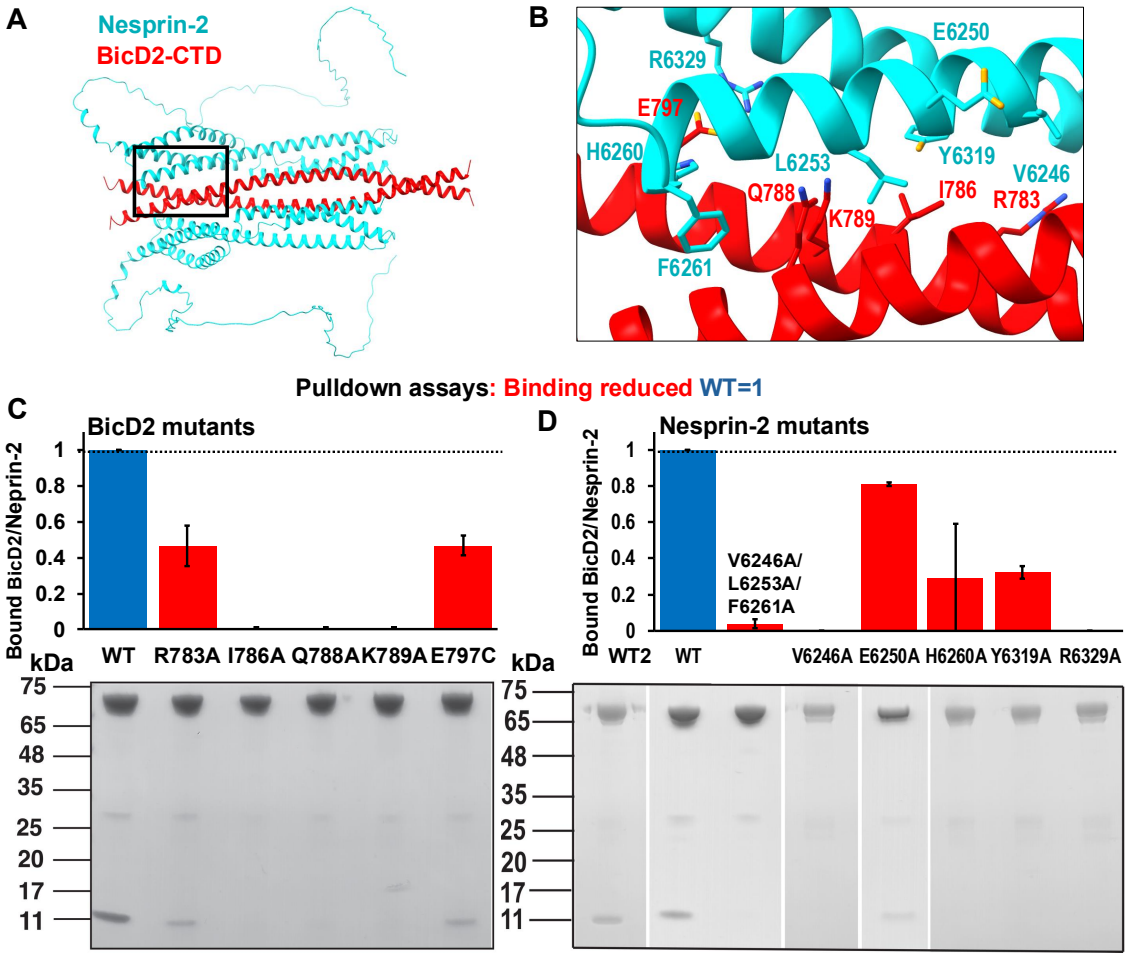

Fig. 4. The structural model of the minimal Nesprin-2/BicD2 complex was validated by mutagenesis and binding assays. (A) Structural model of the minimal Nesprin-2/BicD2 complex. The boxed region is enlarged in B. (B) The Nesprin-2 (cyan) and BicD2 (red) contact residues from the AlphaFold model that were validated by mutagenesis in C and D are shown in stick representation and labelled. (C) BicD2 residues that formed contacts with Nesprin-2 in the structural model were mutated to alanine and the interaction was probed by pulldown-assays. The elution fractions were analyzed by SDS-PAGE and the ratio of bound BicD2-CTD per Nesprin-2 (aa 6123-6421) was quantified from the intensity of the gel bands, and normalized respective to the WT (WT=1). Bar graphs of the ratio of bound BicD2/Nesprin-2 from three experiments and the standard deviation are shown (blue: WT; red: mutants with reduced binding). The SDS-PAGE of the elution fractions of one respective experiment is shown below the bar graph. (D) Nesprin-2 residues that formed contacts with BicD2-CTD were mutated and analyzed as described in C.

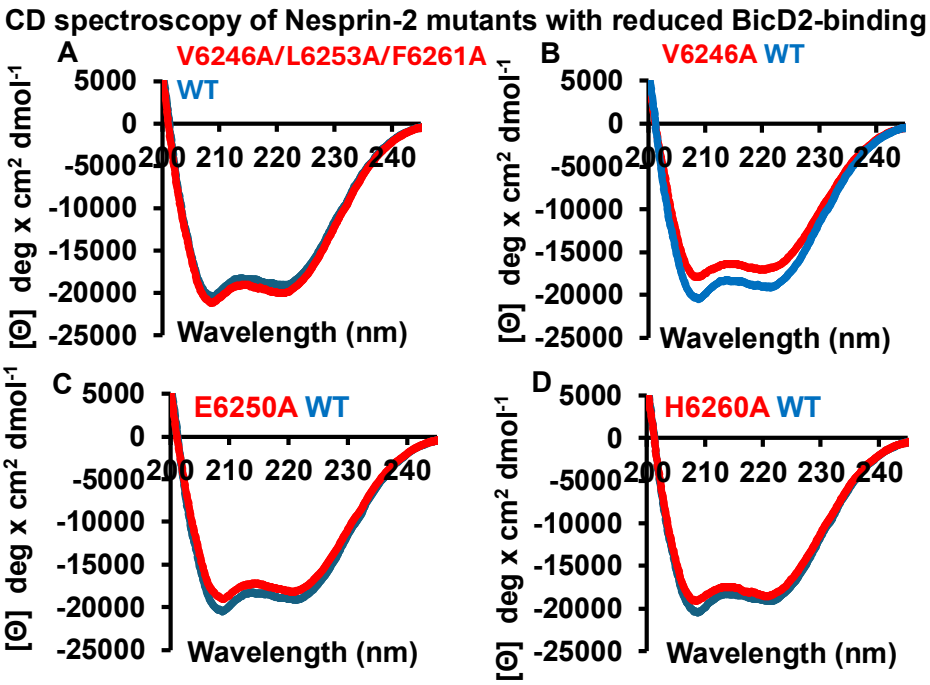

Fig. 5. Circular dichroism (CD) wavelength scans of Nesprin-2 mutants with reduced BicD2 binding are comparable to wild-type (WT) spectra, suggesting the mutations do not induce major structural changes. (A-D) The CD wavelength scans of four purified Nesprin-2 (aa 6123-6421) mutants that reduce binding to BicD2 from Fig. 4 D are shown in red and overlaid with the CD wavelength scan of the WT (blue). The molar ellipticity [θ] is plotted versus the wavelength. The experiment was repeated twice, and a representative experiment is shown.

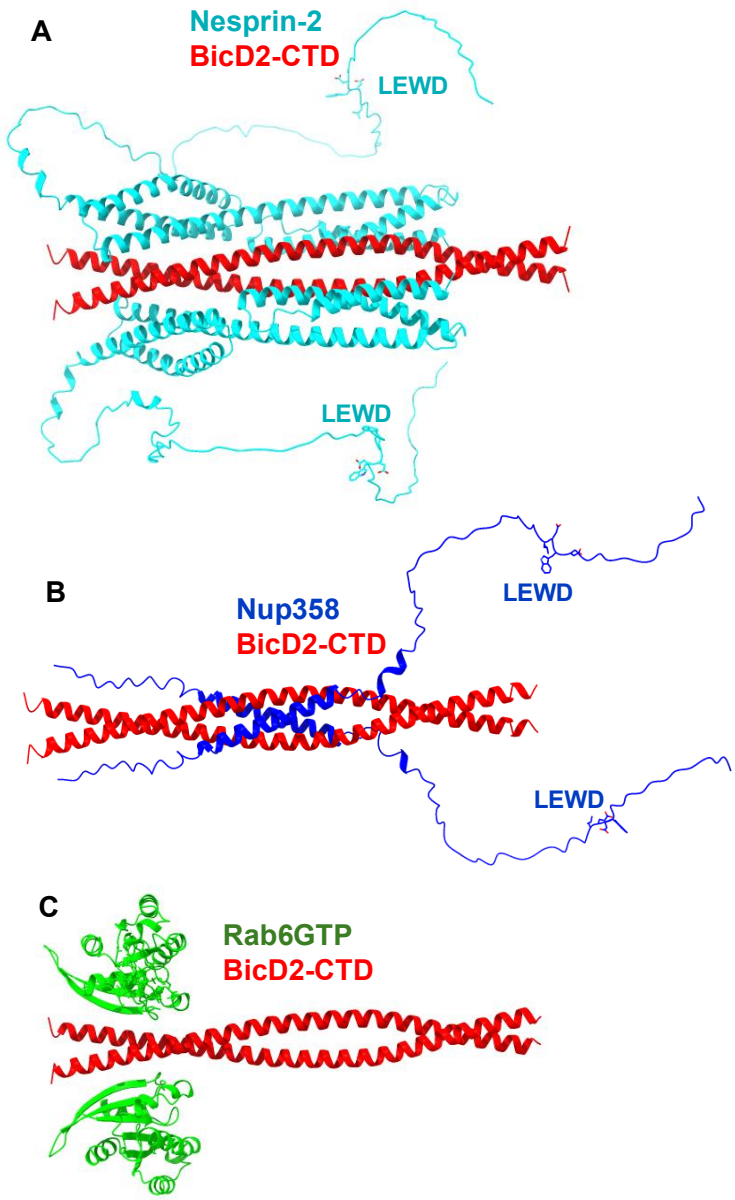

Fig. 6. Cargoes bind to distinct but overlapping sites on BicD2-CTD. (A-C) The experimentally validated structural models of three minimal BicD2/cargo complexes are shown in cartoon representation, with BicD2-CTD in red (Gibson et al., 2022, 2023; Noell et al., 2019; Zhao et al., 2024). (A) Nesprin-2/BicD2 (Nesprin-2: cyan). (B) Nup358/BicD2 (Nup358: blue) (Gibson et al., 2022, 2023). (C) Rab6^{GTP}/BicD2 (Rab6^{GTP}: green) (Zhao et al., 2024). Note that Nup358 and Nesprin-2 have LEWD sequence motifs, which are shown in stick representation and labelled.

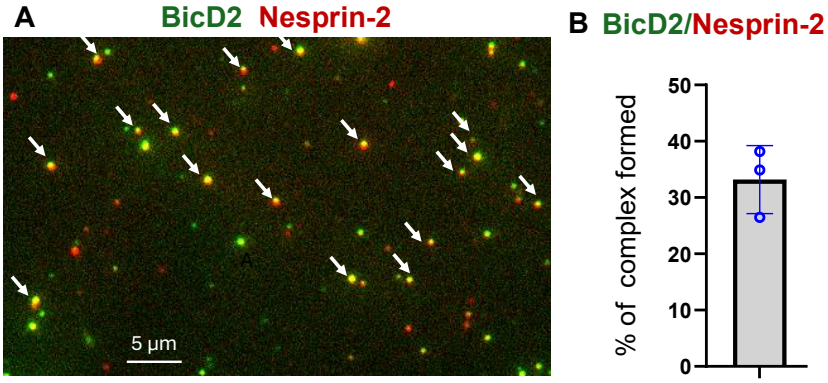

Fig. 7. Minimal Nesprin-2 fragment interacts with full-length BicD2. (A) Full-length BicD2 (labeled with Alexa Fluor 647, red) and minimal Nesprin-2 fragment (aa 6123 - 6352, labeled with Alexa Fluor 488, green) interact, as indicated by yellow colocalized spots (white arrows). (B) Quantification of the Nesprin-2/BicD2 co-localization. Data were collected from three independent experiments.

REFERENCES

Arsenovic, P. T., Ramachandran, I., Bathula, K., Zhu, R., Narang, J. D., Noll, N. A., Lemmon, C. A., Gundersen, G. G., & Conway, D. E. (2016). Nesprin-2G, a Component of the Nuclear LINC Complex, Is Subject to Myosin-Dependent Tension. *Biophysical Journal*, *110*(1), 34–43. https://doi.org/https://doi.org/10.1016/j.bpj.2015.11.014

Brault, J.-B., Bardin, S., Lampic, M., Carpentieri, J. A., Coquand, L., Penisson, M., Lachuer, H., Victoria, G. S., Baloul, S., El Marjou, F., Boncompain, G., Miserey-Lenkei, S., Belvindrah, R., Fraisier, V., Francis, F., Perez, F., Goud, B., & Baffet, A. D. (2022). RAB6 and dynein drive post-Golgi apical transport to prevent neuronal progenitor delamination. *EMBO Reports*, *23*(10), e54605. https://doi.org/10.15252/embr.202254605

Cui, H., Ali, M. Y., Goyal, P., Zhang, K., Loh, J. Y., Trybus, K. M., & Solmaz, S. R. (2020). Coiled-coil registry shifts in the F684I mutant of Bicaudal D result in cargo-independent activation of dynein motility. *Traffic (Copenhagen, Denmark)*, *21*(7), 463–478. https://doi.org/10.1111/tra.12734

Cui, H., Noell, C. R., Behler, R. P., Zahn, J. B., Terry, L. R., Russ, B. B., & Solmaz, S. R. (2019). Adapter Proteins for Opposing Motors Interact Simultaneously with Nuclear Pore Protein Nup358. *Biochemistry*, *58*(50), 5085–5097. https://doi.org/10.1021/acs.biochem.9b00907

Dharan, A., Opp, S., Abdel-Rahim, O., Keceli, S. K., Imam, S., Diaz-Griffero, F., & Campbell, E. M. (2017). Bicaudal D2 facilitates the cytoplasmic trafficking and nuclear import of HIV-1 genomes during infection. *Proceedings of the National Academy of Sciences of the United States of America*, *114*(50), E10707–E10716. https://doi.org/10.1073/pnas.1712033114

Dodding, M. P., Mitter, R., Humphries, A. C., & Way, M. (2011). A kinesin-1 binding motif in vaccinia virus that is widespread throughout the human genome. *The EMBO Journal*, *30*(22), 4523–4538. https://doi.org/10.1038/emboj.2011.326

Evans, R., O'Neill, M., Pritzel, A., Antropova, N., Senior, A., Green, T., Žídek, A., Bates, R., Blackwell, S., Yim, J., Ronneberger, O., Bodenstein, S., Zielinski, M., Bridgland, A., Potapenko, A., Cowie, A., Tunyasuvunakool, K., Jain, R., Clancy, E., … Hassabis, D. (2022). Protein complex prediction with AlphaFold-Multimer. *BioRxiv*, 2021.10.04.463034. https://doi.org/10.1101/2021.10.04.463034

Fridolfsson, H. N., Ly, N., Meyerzon, M., & Starr, D. A. (2010). UNC-83 coordinates kinesin-1 and dynein activities at the nuclear envelope during nuclear migration. *Developmental Biology*, *338*(2), 237–250. https://doi.org/https://doi.org/10.1016/j.ydbio.2009.12.004

Gibson, J. M., Cui, H., Ali, M. Y., Zhao, X., Debler, E. W., Zhao, J., Trybus, K. M., Solmaz, S. R., & Wang, C. (2022). Coil-to-α-helix transition at the Nup358-BicD2 interface activates BicD2 for dynein recruitment. *ELife*, *11*, e74714. https://doi.org/10.7554/eLife.74714

Gibson, J. M., Zhao, X., Ali, M. Y., Solmaz, S. R., & Wang, C. (2023). A structural model for the core Nup358-BicD2 interface. *Biomolecules*, *13*(10), 1445. https://doi.org/10.3390/biom13101445

Gonçalves, J. C., Dantas, T. J., & Vallee, R. B. (2019). Distinct roles for dynein light intermediate chains in neurogenesis, migration, and terminal somal translocation. *The Journal of Cell Biology*, *218*(3), 808–819. https://doi.org/10.1083/jcb.201806112

Gonçalves, J. C., Quintremil, S., Yi, J., & Vallee, R. B. (2020). Nesprin-2 Recruitment of BicD2 to the Nuclear Envelope Controls Dynein/Kinesin-Mediated Neuronal Migration in Vivo. *Current Biology*, *30*(16), 3116-3129.e4. https://doi.org/10.1016/j.cub.2020.05.091

Grigoriev, I., Splinter, D., Keijzer, N., Wulf, P. S., Demmers, J., Ohtsuka, T., Modesti, M., Maly, I. V, Grosveld, F., Hoogenraad, C. C., & Akhmanova, A. (2007). Rab6 Regulates Transport and Targeting of Exocytotic Carriers. *Developmental Cell*, *13*(2), 305–314. https://doi.org/10.1016/j.devcel.2007.06.010

Hoogenraad, C. C., Akhmanova, A., Howell, S. A., Dortland, B. R., De Zeeuw, C. I., Willemsen, R., Visser, P., Grosveld, F., & Galjart, N. (2001). Mammalian Golgi-associated Bicaudal-D2 functions in the dynein-dynactin pathway by interacting with these complexes. *EMBO J*, *20*(15), 4041–4054. https://doi.org/10.1093/emboj/20.15.4041

Hoogenraad, C. C., Wulf, P., Schiefermeier, N., Stepanova, T., Galjart, N., Small, J. V., Grosveld, F., de Zeeuw, C. I., & Akhmanova, A. (2003). Bicaudal D induces selective dynein-mediated microtubule minus end-directed transport. *EMBO J*, *22*(22), 6004–6015. https://doi.org/10.1093/emboj/cdg592

Hu, D. J.-K., Baffet, A. D., Nayak, T., Akhmanova, A., Doye, V., & Vallee, R. B. (2013). Dynein recruitment to nuclear pores activates apical nuclear migration and mitotic entry in brain progenitor cells. *Cell*, *154*(6), 1300–1313. https://doi.org/10.1016/j.cell.2013.08.024

Jumper, J., Evans, R., Pritzel, A., Green, T., Figurnov, M., Ronneberger, O., Tunyasuvunakool, K., Bates, R., Žídek, A., Potapenko, A., Bridgland, A., Meyer, C., Kohl, S. A. A., Ballard, A. J., Cowie, A., Romera-Paredes, B., Nikolov, S., Jain, R., Adler, J., … Hassabis, D. (2021). Highly accurate protein structure prediction with AlphaFold. *Nature*, *596*(7873), 583–589. https://doi.org/10.1038/s41586-021-03819-2

Krissinel, E., & Henrick, K. (2007). Inference of macromolecular assemblies from crystalline state. *Journal of Molecular Biology*, *372*(3), 774–797. https://doi.org/10.1016/j.jmb.2007.05.022

Manigrasso, G., Saharat, K., Kullapanich, C., Buolanger, J., Morgan, T. E., Kramer, H., Salje, J., & Carter, A. P. (2024). The intracellular bacterium Orientia tsutsugamushi hijacks the adaptor protein BICD2 for dynein-based motility. *BioRxiv*, 2024.04.11.589026. https://doi.org/10.1101/2024.04.11.589026

Matanis, T., Akhmanova, A., Wulf, P., Del Nery, E., Weide, T., Stepanova, T., Galjart, N., Grosveld, F., Goud, B., De Zeeuw, C. I., Barnekow, A., & Hoogenraad, C. C. (2002). Bicaudal-D regulates COPI-independent Golgi–ER transport by recruiting the dynein–dynactin motor complex. *Nature Cell Biology*, *4*(12), 986–992. https://doi.org/10.1038/ncb891

McGee, M. D., Rillo, R., Anderson, A. S., & Starr, D. A. (2006). UNC-83 Is a KASH Protein Required for Nuclear Migration and Is Recruited to the Outer Nuclear Membrane by a Physical Interaction with the SUN Protein UNC-84. *Molecular Biology of the Cell*, *17*(4), 1790–1801. https://doi.org/10.1091/mbc.e05-09-0894

McKenney, R. J., Huynh, W., Tanenbaum, M. E., Bhabha, G., & Vale, R. D. (2014). Activation of cytoplasmic dynein motility by dynactin-cargo adapter complexes. *Science (New York, N.Y.)*, *345*(6194), 337–341. https://doi.org/10.1126/science.1254198

Micsonai, A., Moussong, É., Wien, F., Boros, E., Vadászi, H., Murvai, N., Lee, Y.-H., Molnár, T., Réfrégiers, M., Goto, Y., Tantos, Á., & Kardos, J. (2022). BeStSel: webserver for secondary structure and fold prediction for protein CD spectroscopy. *Nucleic Acids Research*, *50*(W1), W90–W98. https://doi.org/10.1093/nar/gkac345

Mirdita, M., Schütze, K., Moriwaki, Y., Heo, L., Ovchinnikov, S., & Steinegger, M. (2022). ColabFold: making protein folding accessible to all. *Nature Methods*, *19*(6), 679–682. https://doi.org/10.1038/s41592-022-01488-1

Noell, C. R., Loftus, K. M., Cui, H., Grewer, C., Kizer, M., Debler, E. W., & Solmaz, S. R. (2018). A Quantitative Model for BicD2/Cargo Interactions. *Biochemistry*, *57*(46), 6538–6550. https://doi.org/10.1021/acs.biochem.8b00987

Noell, C. R., Loh, J. Y., Debler, E. W., Loftus, K. M., Cui, H., Russ, B. B., Zhang, K., Goyal, P., & Solmaz, S. R. (2019). Role of Coiled-Coil Registry Shifts in the Activation of Human Bicaudal D2 for Dynein Recruitment upon Cargo Binding. *The Journal of Physical Chemistry Letters*, *10*(15), 4362–4367. https://doi.org/10.1021/acs.jpclett.9b01865

Peeters, K., Chamova, T., & Jordanova, A. (2014). Clinical and genetic diversity of SMN1-negative proximal spinal muscular atrophies. *Brain : A Journal of Neurology*, *137*(Pt 11), 2879–2896. https://doi.org/10.1093/brain/awu169

Pettersen, E. F., Goddard, T. D., Huang, C. C., Meng, E. C., Couch, G. S., Croll, T. I., Morris, J. H., & Ferrin, T. E. (2021). UCSF ChimeraX: Structure visualization for researchers, educators, and developers. *Protein Science : A Publication of the Protein Society*, *30*(1), 70–82. https://doi.org/10.1002/pro.3943

Rossor, A. M., Sleigh, J. N., Groves, M., Muntoni, F., Reilly, M. M., Hoogenraad, C. C., & Schiavo, G. (2020). Loss of BICD2 in muscle drives motor neuron loss in a developmental form of spinal muscular atrophy. *Acta Neuropathologica Communications*, *8*(1), 34. https://doi.org/10.1186/s40478-020-00909-6

Schlager, M. A., Hoang, H. T., Urnavicius, L., Bullock, S. L., & Carter, A. P. (2014). In vitro reconstitution of a highly processive recombinant human dynein complex. *The EMBO Journal*, *33*(17), 1855–1868. https://doi.org/10.15252/embj.201488792

Schneider, C. A., Rasband, W. S., & Eliceiri, K. W. (2012). NIH Image to ImageJ: 25 years of image analysis. *Nature Methods*, *9*(7), 671–675. https://doi.org/10.1038/nmeth.2089

Serra-Marques, A., Martin, M., Katrukha, E. A., Grigoriev, I., Peeters, C. A. E., Liu, Q., Hooikaas, P. J., Yao, Y., Solianova, V., Smal, I., Pedersen, L. B., Meijering, E., Kapitein, L. C., & Akhmanova, A. (2020). Concerted action of kinesins KIF5B and KIF13B promotes efficient secretory vesicle transport to microtubule plus ends. *ELife*, *9*, e61302. https://doi.org/10.7554/eLife.61302

Splinter, D., Tanenbaum, M. E., Lindqvist, A., Jaarsma, D., Flotho, A., Yu, K. Lou, Grigoriev, I., Engelsma, D., Haasdijk, E. D., Keijzer, N., Demmers, J., Fornerod, M., Melchior, F., Hoogenraad, C. C., Medema, R. H., & Akhmanova, A. (2010). Bicaudal D2, dynein, and kinesin-1 associate with nuclear pore complexes and regulate centrosome and nuclear positioning during mitotic entry. *PLoS Biology*, *8*(4), e1000350–e1000350. https://doi.org/10.1371/journal.pbio.1000350

Will, L., Portegies, S., van Schelt, J., van Luyk, M., Jaarsma, D., & Hoogenraad, C. C. (2019). Dynein activating adaptor BICD2 controls radial migration of upper-layer cortical neurons in vivo. *Acta Neuropathologica Communications*, *7*(1), 162. https://doi.org/10.1186/s40478-019-0827-y

Wilson, M. H., & Holzbaur, E. L. F. (2012). Opposing microtubule motors drive robust nuclear dynamics in developing muscle cells. *Journal of Cell Science*, *125*(Pt 17), 4158–4169. https://doi.org/10.1242/jcs.108688

Wilson, M. H., & Holzbaur, E. L. F. (2015). Nesprins anchor kinesin-1 motors to the nucleus to drive nuclear distribution in muscle cells. *Development (Cambridge, England)*, *142*(1), 218–228. https://doi.org/10.1242/dev.114769

Yi, J., Zhao, X., Noell, C. R., Helmer, P., Solmaz, S. R., & Vallee, R. B. (2023). Role of Nesprin-2 and RanBP2 in BICD2-associated brain developmental disorders. *PLoS Genetics*, *19*(3), e1010642. https://doi.org/10.1371/journal.pgen.1010642

Zhang, Q., Bethmann, C., Worth, N. F., Davies, J. D., Wasner, C., Feuer, A., Ragnauth, C. D., Yi, Q., Mellad, J. A., Warren, D. T., Wheeler, M. A., Ellis, J. A., Skepper, J. N., Vorgerd, M., Schlotter-Weigel, B., Weissberg, P. L., Roberts, R. G., Wehnert, M., & Shanahan, C. M. (2007). Nesprin-1 and -2 are involved in the pathogenesis of Emery–Dreifuss muscular dystrophy and are critical for nuclear envelope integrity. *Human Molecular Genetics*, *16*(23), 2816–2833. https://doi.org/10.1093/hmg/ddm238

Zhang, X., Lei, K., Yuan, X., Wu, X., Zhuang, Y., Xu, T., Xu, R., & Han, M. (2009a). SUN1/2 and Syne/Nesprin-1/2 complexes connect centrosome to the nucleus during neurogenesis and neuronal migration in mice. *Neuron*, *64*(2), 173–187. https://doi.org/10.1016/j.neuron.2009.08.018

Zhang, X., Lei, K., Yuan, X., Wu, X., Zhuang, Y., Xu, T., Xu, R., & Han, M. (2009b). SUN1/2 and Syne/Nesprin-1/2 Complexes Connect Centrosome to the Nucleus during Neurogenesis and Neuronal Migration in Mice. *Neuron*, *64*(2), 173–187. https://doi.org/10.1016/j.neuron.2009.08.018

Zhao, X., Quintremil, S., Rodriguez Castro, E. D., Cui, H., Moraga, D., Wang, T., Vallee, R. B., & Solmaz, S. R. (2024). Molecular mechanism for recognition of the cargo adapter Rab6GTP by the dynein adapter BicD2. *Life Science Alliance*, *7*(7), e202302430. https://doi.org/10.26508/lsa.202302430

Zhou, C., Wu, Y. K., Ishidate, F., Fujiwara, T. K., & Kengaku, M. (2024). Nesprin-2 coordinates opposing microtubule motors during nuclear migration in neurons. *Journal of Cell Biology*, *223*(11), e202405032. https://doi.org/10.1083/jcb.202405032

Zhu, R., Antoku, S., & Gundersen, G. G. (2017). Centrifugal Displacement of Nuclei Reveals Multiple LINC Complex Mechanisms for Homeostatic Nuclear Positioning. *Current Biology : CB*, *27*(20), 3097-3110.e5. https://doi.org/10.1016/j.cub.2017.08.073